Title
Near-Infrared Observations of the Environments of Radio-quiet QSOs at $z \gtrsim 1$

Journal
The Astrophysical Journal, 520(2)

ISSN
0004-637X

Authors
Teplitz, Harry I
McLean, Ian S
Malkan, Matthew A

Publication Date
1999-08-01

DOI
10.1086/307480

Peer reviewed

Near-Infrared Observations of the Environments of Radio Quiet QSOs at z$\gtrsim$1

Harry I. Teplitz [1] [2]
Goddard Space Flight Center, Code 681, GSFC, Greenbelt, MD 20771
hit@binary.gsfc.nasa.gov

Ian S. McLean, Matthew A. Malkan
Department of Physics & Astronomy, Division of Astronomy
University of California at Los Angeles
Los Angeles, CA 90095-1562
malkan@astro.ucla.edu, mclean@astro.ucla.edu

ABSTRACT

We present the results of an infrared survey of QSO fields at z=0.95, 0.995 and 1.5. Each $z < 1$ field was imaged to typical continuum limits of J=20.5, K′=19 (5σ), and line fluxes of 1.3×10^{-16} ergs/cm^2/s (1σ) in a 1% interference filter. 16 fields were chosen with $z \sim 0.95$ targets, 14 with $z \sim 0.995$ and 6 with $z \sim 1.5$. A total area of 0.05 square degrees was surveyed, and two emission-line objects were found. We present the infrared and optical photometry of these objects. Optical spectroscopy has confirmed the redshift of one object (at z=0.989) and is consistent with the other object having a similar redshift. We discuss the density of such objects across a range of redshifts from this survey and others in the literature. We also present number-magnitude counts for galaxies in the fields of radio quiet QSOs, supporting the interpretation that they exist in lower density environments than their radio loud counterparts. The J-band number counts are among the first to be published in the J=16–20 range.

Subject headings: galaxies : individual — galaxies : evolution — cosmology : observation — infrared : galaxies

---

[1]NOAO Research Associate

[2]Previous affiliation: Department of Physics & Astronomy, UCLA

1. Introduction

Current estimates of the global star formation rate show a steep rise in activity out to a redshift of 1 (Lilly et al. 1996). Half of the stars in the current universe may have formed since z=1. High redshift star-forming galaxies are also seen to be highly biased tracers of the mass distribution of the universe (Steidel et al. 1998). As a result of these two observations, significant effort has been devoted in recent years to the search for galaxy clusters at redshifts beyond z=1 (Dickinson 1997, Donahue et al. 1998, etc.) Narrow-band searches for the Hα emission line have successfully identified star forming galaxies at $z > 2$ (Malkan, Teplitz & McLean 1995, 1996; Teplitz, Malkan, & McLean 1998, hereafter TMM98; and Mannucci, Thompson, Beckwith, and Williger 1998, hereafter MTBW98), and searches for [OII] and [OIII] have been used at $z \sim 0.9$ (MTBM98) and $z > 3$ (Teplitz, Malkan, and McLean 1999; hereafter TMM99). In this paper we apply this imaging infrared technique to the search for $z \sim 1$ galaxies.

It takes patience to find the relatively rare galaxies at z=1 simply by covering large areas of random field. Instead, we have chosen the popular tactic of looking for galaxies where they are most likely to be: near other galaxies or QSOs. In particular, we search fields containing radio-loud or radio-quiet quasars, and fields containing absorption line systems in QSO lines of sight. All of these objects have previously been associated with the presence of groups of galaxies.

Yee & Green (1987) and later Ellingson, Yee, & Green (1991) have examined galaxy clusters as the environment of quasars, though their searches extend only out to z=0.7. They find significantly more bright QSOs in clusters at higher redshifts, indicating that quasars may be good markers of galaxy clusters. Similarly, large numbers of excess galaxies were found in Radio Loud QSO fields at $1 < z < 2$ by Hall & Green (1998; see also Hall, Green & Cohen 1998). At $z \sim 2$, Aragón-Salamanca et al. (1996) find an excess of K-band selected galaxies in the environments of QSOs. Also at $z > 2$, Hutchings (1995) finds excess R-band selected galaxies in the fields of both radio-loud and radio-quiet QSOs. In similar searches, high redshift radio galaxies are also seen as markers of other clustered galaxies (Dickinson 1997).

Absorption-line systems have also been studied in detail for their galaxy content. Galaxies have been identified as responsible for Mg II and C IV absorption out to $z \sim 1$ (*e.g.* Steidel et al., 1997). Aragón-Salamanca et al. (1994) have demonstrated excess K-selected galaxies in fields containing C IV absorbers. Possible Damped Lyα Absorption (DLA) systems have been identified past $z = 3$ (Djorgovski 1996, Moller & Warren 1998). The presence of galaxies as the absorbers make such systems good markers for other galaxies. However, the small impact parameters will often make the absorbers themselves

hard to see except with very high resolution.

We have chosen to search for Hα as an indicator of star formation in normal galaxies. It is strong in nearby spirals, with equivalent widths of 50Å or more in the actively star-forming galaxies (Kennicutt, 1983). There are several methods of identifying on-going star formation, and determining the Star Formation Rate (SFR) with various degrees of accuracy. Emission may either be observed from the UV continuum of young stars, from the ionized gas in HII regions, or re-radiated in the FIR by dust. Hα emission, at 6563Å, can be observed from nebular emission in the star-forming HII regions. This emission line has the advantage of relatively long wavelength, making it less susceptible to extinction than the UV continuum. There is a concern that the emission actually observed is a combination of lines, but the [N II] 6584Å line is found to be weak in most cases, at most 10–30% of Hα (Kennicutt & Kent, 1983).

Kennicutt (1983) calculates the SFR based on Hα luminosity to be

$$\mathrm{SFR(total)} = \frac{L(\mathrm{H}\alpha)}{1.12 \times 10^{41} \mathrm{ergs\ s^{-1}}} \mathrm{M_\odot yr^{-1}} \tag{1}$$

for an Initial Mass Function (IMF) that is effectively that of Salpeter, with $\psi(m) \propto m^{-2.5}$, and an upper mass cutoff of $100\mathrm{M}_\odot$. Similar estimates can be made from observations of the O II emission line (Kennicutt 1992, but see Hammer et al., 1997).

The Hα emission line has also been used to measure the SFR in high redshift galaxies selected by other methods. For example, Glazebrook et al. (1998) have spectroscopically measured Hα in 13 $z \sim 1$ galaxies selected from the Canda-France Redshift Survey (see Lilly et al. 1996). They find that $z \sim 1$ galaxies may have SFRs three times higher than would be inferred from rest-frame UV observations.

2. Observations

All IR observations in the $z \sim 1$ survey were taken on the Shane 3m telescope at Lick Observatory on Mount Hamilton, with the UCLA Two Channel Near-IR Camera, colloquially known as "Gemini" for its twin detectors, (McLean, 1994). Use of this instrument for deep IR imaging has been discussed in McLean & Teplitz (1997; hereafter MT97) and Larson et al. (1997). The observations of the six $z \sim 1.5$ fields were taken at the 10m Keck I telescope using the Near IR Camera, NIRC (Matthews et al., 1994). For a discussion of filter transmission in the NIRC instrument see TMM98.

The UCLA 2-Channel Near-IR Camera (see also McLean et al., 1993, 1994) has two independent infrared arrays, one 256×256 pixel NICMOS 3 HgCdTe device and

one 256 × 256 pixel SBRC InSb detector. The camera is a low-noise, high-throughput system. To optimize performance, the instrument employs a variety of readout modes, including Correlated-Double-Sampling, Fowler Sampling (see Fowler & Gatley 1990), a multiple-reads-per-pixel mode, and subarray readouts. Typical deep integrations, like those we employ in this project, utilize Fowler sampling, with 8–32 multiple reads. The plate scale for the detectors is 0.70″and $\sim$ 0.68″/ pixel for the short- and long-wavelength channels. These scales correspond to a field of view of $\sim 3' \times 3'$. We chose a dichroic beam splitter which directs light longward of 2 μm to the SBRC array. Our typical exposure times were three coadds of 50 seconds each in the J band, 18 coadds of 8 seconds in K′, and a single 240 second exposure in the narrow band.

Each channel has a filter wheel containing 25.4 mm diameter transmission and blocking filters. In addition to the standard J,H, and K′ filters, this project utilized two narrow-band interference filters. The filters were purchased from Barr Associates in Westford, Massachusetts. One was "off the shelf", while the other was custom made for this project. Table 1 summarizes the properties of each filter, as described below. The first narrow-band filter is the standard filter at 1.28 μm, usually used to measure the Paschen β (Pβ) transition. It is 141Å wide, which corresponds to $\Delta\lambda/\lambda = 1.1\%$. Standard star observations show that the ratio of Pβ filter transmission to standard J filter transmission is $1 : 22 \pm 1$. The wavelength of the Pβ filter corresponds to the redshifted wavelength of Hα at at $z = 0.95$.

The second narrow band filter was custom-designed for this project. The filter is centered on 1.3095 μm, to probe a redshift range higher than that of the Pβ filter. The choice was constrained by the atmospheric absorption at the red end of the J passband. At $z = 0.995$, Hα redshifts into this filter. The filter was produced using a new oxide manufacturing process, in order to maximize throughput and cryogenic performance. The filter transmission is fairly flat around the peak of 78%, centered on 1.3095 μm, with a width of 0.0130 μm, as verified in a cryogenic test. The transmission was confirmed by standard star observations which show that the ratio of transmitted flux compared to the J filter is $1 : 19 \pm 1$.

Targets were selected from a search of NASA/IPAC Extragalactic Database, in fields containing QSOs (either radio loud and radio quiet) or absorption line systems (either DLA or or metal line absorbers). Objects below -30° were not considered as Keck targets, nor south of -5° as Lick targets. Subject to these constraints, we then selected fields at redshifts within $\pm 0.3\%$ of the central redshift of the filters.

The data were reduced following the procedures outlined in TMM98 and MT97 which will only be summarized here. We obtained images in a sequence of "dithered" exposures,

offsetting the telescope between exposures in a 3×3 grid typically spaced by 10–20 pixels. The individual frames were divided by a twilight flat or dome flat (as available). Then a running median sky frame (created from the nine exposures taken closest in time to each image) was subtracted. When no such flat was available, the running median was divided into each image and sky subtraction was left to aperture photometry. Objects were identified using the SExtractor (Bertin & Arnouts 1996) software. Photometry was performed using apertures of 2.5 times the seeing disk. The same aperture was applied to broad and narrow-band exposures. Similarly, the same photometric aperture was applied to both J and K′ frames. Photometric errors were estimated from aperture photometry performed on random positions in the frame. Errors in the narrow-minus-broad band color were estimated from a Monte Carlo simulation of the ratio of numbers with large gaussian errors in order to define the confidence intervals. (See TMM98 for details).

Follow-up optical imaging and spectroscopy was obtained with the Low Resolution Imaging Spectrometer (LRIS), which has a 2048×2048 pixel CCD detector, with a field of view of 5′ by 7′ (Oke et al., 1995). Spectra were taken with the 300 lines/mm grating, giving a dispersion of 2.48Å pixel^{-1}, and spectral resolution (FWHM) of 4.5 pixels. These data were reduced with standard IRAF procedures.

3. Results

There were 43 known targets meeting our criteria. Of these possible fields, we imaged 30 during the 11 clear nights available for this project (see Table 2). Table 3 lists QSO photometry for each field, and estimated optical magnitudes from the NED database. In each field, we obtained simultaneous J and K′ imaging at integration times designed to detect ∼L* galaxies at the appropriate redshifts. Fields observed at high signal-to-noise or that seemed otherwise promising were planned for narrow-band followup. Table 4 lists narrow band observations and inferred limiting SFR. Six fields observed with z=1.5 "signposts" are also listed in Table 5.

3.1. Discussion of Individual Fields

In each field, the errors in the Broad–Narrow colors were calculated as discussed, above. Objects with narrow-band excesses lying at above the 99% confidence interval are considered possible detections. Two apparent Hα-emitters were detected in this survey. They are listed in Table 6, along with their inferred SFR and broad-band photometry.

Our detection limits were typically J=20.5 (5σ) and SFR = 12 $M_\odot yr^{-1}(2\sigma)$. This depth should be sufficient to pick up vigorously star forming galaxies at z=1. The GISSEL96 (see Bruzual & Charlot 1993) models predict that an evolved L* galaxy at z=1 will have J=20.5. Adding a strong ongoing episode of star formation encompassing 10% of the galaxy's mass over 1Gyr would lead to a SFR=$10M_\odot yr^{-1}$.

The survey has covered approximately 190 square arcminutes (in the highest SNR regions). This is sufficient to constrain the size of a moderately high-redshift galaxy population with SFR's at the sensitivities we have achieved.

0107-025

This field was of particular interest because there are two known QSOs within one UCLA Camera field of view with emission redshifts that place Hα in the Pβ filter (see Figure 1). However no new line-emitting objects were detected. The two QSOs are clearly detected in the narrow band. Figure 2 compares the number of galaxies in this field to the average J number counts for all the broad band fields. Since little J-band field data are availabe at these magnitudes (see Section 5), we use our averaged number counts. There is a possible excess in several bins at $J > 19$, about 1σ above the average per bin.

2145+067

Figure 3 shows the broad-band image of this field. No statistical excess of galaxies has been detected (see Figure 4). A drawback to its consideration as a target is the bright star in the southern region of the field. As a result, we decided against it in the first set of narrow-band observations in August of 1995. However, we did select it as a target the following year, and observed it in October, 1996.

One object in this field shows an apparent $\sim 3\sigma$ excess in the narrow band filter (see Figure 5). Its Δm= 1.2 yields an inferred SFR=$53M_\odot$/yr, assuming the line is Hα at $z = 0.995$. The inferred equivalent width would be 132Å or 2% EW/λ. The object lies $45''$ from the QSO. It has a FWHM of $4.2''$, compared to a seeing disk of $2.2''$. Our photometry shows the galaxy to have $I = 22.5$, $J = 19.2$, and K′= 18.6. Optical CCD imaging of this field as a followup of HST QSO fields (Kirhakos et al., 1994) did not detect this object, down to a limit of $g \sim= 22$, consistent with our I band detection. These colors are generally consistent with a $z \sim 1$ galaxy, where the 4000/3646Å break lies in the I band. Assuming passive evolution, this galaxy would be somewhat brighter than L_* today.

The line-emitting galaxy in this field is located 14″ west of a bright star. This initially suggested that the detection could actually be a ghost. To test this, an image was taken through the same filter of a bright star in a relatively uncrowded field. Two ghosts were identified to the SE of the star, as a distinctive "double". No ghost image was detected at the position of the possible Hα-emitter. Also, the strong detection of the object in both the J and Pβ filters makes the risk of a ghost less likely.

We subsequently detected this object with LRIS imaging and spectroscopy, demonstrating that it is real and not a ghost. We do not find any emission lines to confirm the object's redshift. In a future paper, we will present an analysis of cross-correlation of this spectrum with galaxy spectra at various redshifts (see also Cohen et al. 1998).

LBQS 2350-0132

A single, strong Hα-emitting object is detected in this field (see Figures 6 and 7). It is shows Hα emission with an EW of 1.3%, or SFR=26.0$M_\odot yr^{-1}$. The line flux is 5.1×10^{-16}ergs/cm^2/sec., and the equivalent width is 86Å in the restframe. The object is clearly extended with FWHM=3.0″ compared to a seeing disk of 1.5″. It lies 47″ from the QSO (400kpc at z=0.993).

The J-K′=1.3 color of this object is blue for an evolved elliptical at this redshift, but could be consistent with a starburst. Its K′ continuum magnitude is roughly consistent with an L* galaxy at this redshift, suggesting that this is a secondary starburst, not the initial formation of the galaxy. Photometry with LRIS shows the galaxy to have $I = 21.9$, still fairly blue for galaxies at that redshift. This same field was observed by Kirhakos et al.(1994). They do not detect this object down to a limit of $g \sim 22$, again consistent with our photometry.

The number counts for this field do not show any excess of faint galaxies (see Figure 8). Similarly, the reddest objects in the frame are not clustered near the line-emitter, nor near each other. A single very red object (J-K′=2.8) lies $\sim 45''$ north of the detection, though it falls in a lower SNR region of the image.

We have obtained LRIS imaging and spectroscopy of this field. The redshift inferred for the narrow-band detection is confirmed to be $z = 0.989 \pm 0.001$ by the presence of the [OII] emission line in the optical spectrum (see figure 9). The redshift difference between the QSO and the galaxy (along the line of sight) corresponds to 4.2 Mpc at z=0.99, which is large to suggest no physical connection with the signpost. The [OII] line is unresolved at the resolution of the spectrum, which constrains the intrinsic width to be no greater than

300 km/s. The line flux is 1.9×10^{-16} ergs/cm^2/s. The equivalent width of the [OII] line is 80Å in the restframe, or 93% of the equivalent with of the Hα+NII complex. Kennicutt (1992) finds that most low redshift star forming galaxies have EW([OII]):EW(Hα) ratios of 0.40, though there is considerable scatter for objects with EW(Hα)$>$ 40Å, such as this one. Kennicutt also comments that Seyfert 2 galaxies are found to have high EW([OII]):EW(Hα) ratios while Seyfert 1's have low ratios. Thus it is possible that this candidate object contains a Seyfert 2 nucleus, though the line ratio does not preclude a purely stellar origin. The angular extent of the continuum image argues against a broad-line object (Seyfert 1). Even a narrow-line AGN (Seyfert 2) would be expected to produce some detectable Mg II emission, which should have fallen in a good region of our spectrum, but is not seen. The 3σ limit at the wavelength of redshifted Mg II is 6×10^{-18} ergs/cm^2/sec.

4. Emission Line Galaxies at $z \sim 1$

We have detected one definite and one probable Hα-emitting galaxy at $z \geq 0.95$. This corresponds to a surface density of 0.01 galaxies per square arcminute. For comparison at z=3 in large ($\Delta z > 0.4$) redshift windows, field galaxies are detected, with SFR$\sim 8 M_\odot yr^{-1}$, at 0.4–0.8 per square arcmin (Steidel et al., 1996).

As a volume density, our two detections yield $4.7^{+6}_{-3} \times 10^{-4}$ galaxies/Mpc^3 (comoving). This density is similar to that for field Hα-emitting galaxies at this redshift, as determined by the NICMOS parallel grism survey (McCarthy et al. 1999). Table 7 lists results of various Hα surveys for star-forming galaxies for different redshifts. Comparing the results, we find broad agreement in the densities of Hα-emitters, with a higher density in absorption-line fields, as already noted in TMM98 and MTBW98. We also find good agreement in the average star formation rates at different redshifts. This constant detected average SFR may be the result of the bias imposed by a flux-limited survey (for example TMM98 found fainter, less vigorously star forming objects by going deeper). However, the consistency in the average SFR of galaxies brighter than the flux limit may be indicative of the constant global star formation rate observed at $z > 1$. Lyman Break galaxy searches (Steidel et al. 1998) and observations in the sub-mm (c.f. Smail et al. 1998) have suggested that the global SFR does not change much between redshifts of 1 and 5.

5. Number-Magnitude Counts

Our typical broad-band detection limits are J=20.5 and K′=19.0, corresponding to an evolved L_* galaxy at $z \sim 1$. In Figures 10 and 11 we plot the number-magnitude counts in J and K′. For comparison, the number counts from the literature are also plotted. In both the J and K′ bands, we find no statistical excess of galaxies averaged over the total survey area in QSO fields. It has been suspected for some time that radio-quiet QSOs (RQQs) at most redshifts do not lie in high density environments, unlike radio-loud QSOs (RLQs). Most of the quasars in our sample are RQQs, and so it is perhaps not surprising that our number counts agree with the field. Table 8 lists the number-magnitude counts per square degree per magnitude for the J band.

Our J-band number counts are among the first wide-field number-counts for any environment at deep J magnitudes. The DENIS Survey (Mamon et al., 1998) has provided J-band number counts down to J=15. Deep J-band counts will soon be available from the NICMOS parallel survey (c.f. Teplitz et al. 1998, Yan et al. 1998), and counts at J fainter than 20 have been measured by Bershady et al. 1998. It is of particular interest to have number counts in different IR wavebands, in order to provide good field comparisons for the study of cluster environments at different wavelengths (c.f. Stanford et al. 1997).

Our result that RQQs lie in low density environments is supported by the conclusion reached by Croom & Shanks (1998) for RQQs at $z < 1.5$. They find no significant clustering signal for galaxies down to L_*. Their observations were in the B_j-band, sampling the restframe near-UV, so a K-band survey provides significant new data. Similarly, both TMM98 and Mannucci et al. (1998) find few galaxies associated with $z < 3$ (mostly radio quiet) QSOs.

On the other hand, Jaeger et al. (1999) find a significant excess of galaxies close to RQQs at $z \sim 1$ in R band observations. We can also consider the radial distribution of galaxies in reference to the QSO for our fields in the J band (see Figure 12). This analysis is more sensitive to small scale clustering, that has no impact on the average number counts over then entire area. There is a marginally significant excess of galaxies within $\sim 15''$ of the QSO ($\sim$ 120 kpc at z=1). We note however that there are a total of only 66 galaxies in the three innermost bins, compared with a field expectation of 47 galaxies, or an average excess of one galaxy per two fields. The field expectation the same, whether it is determined from the average number counts over the entire survey area, or from repeating the radial binning around random points in the fields. Such a small possible excess is only present at the $\sim 2\sigma$ level. In addition, even accepting such an excess, it argues for RQQ environments being poor groups of galaxies, not rich cluster. However, the radial extent is generally consistent with the results of TMM98, which found no roll-off in the radial distribution of

Hα-emitters within one NIRC field ($38'' \times 38''$).

The potentially excess galaxies detected in the broad-band, if they are physically associated with the quasar signposts (within 2% of redshift), have a density which is higher than that of strong Hα-emitters. This effect would not be unexpected, if one assumes that there is a large population of less actively star-forming galaxies by a redshift of one. The galaxies around these quasars might be seen to be actively star-forming at a much earlier epoch. For example, Hu et al. (1998) and Djorgovski et al. (1997) find high densities of Lyα-emitters around $z > 4$ QSOs. This could imply that by $z \sim 1$, little active star formation is to be found in poor groups. By contrast, richer groups around QSOs at $z \sim 1.5$ are seen to have a higher density of Hα-emitters (Hall 1998). Indeed, by $z \sim 0.4$, active star-formation is more often observed in rich clusters (see Oemler 1992).

6. Future Prospects

This project has demonstrated that future narrow-band imaging surveys can succeed in probing the $z \geq 1$ Universe, if sufficiently long integration times are combined with new large-format infrared arrays. At that point it will be reasonable to make blind searches of the field, which will reveal if the targeted searches described here have benefited much from galaxy clustering around quasars and their absorbers.

We thank the Telescope Technicians at Lick Observatory and the Observing Assistants and Instrument Specialists at the Keck telescopes. We also thank the members of the UCLA IR Detector Lab, especially J. Canfield and N. Magnone for enabling the many observing runs with the UCLA IR Camera. We thank E. Becklin, B. Zuckerman, and P. Lowrance for aquiring a portion of the data on the 0500+019 field We thank Matthew Bershady and Gary Mamon for making their number counts available to us in electronic form; and Jonathon Gardner and G. Williger for useful discussions.

This research has made use of the NASA/IPAC Extragalactic Database (NED) which is operated by the Jet Propulsion Laboratory, California Institute of Technology, under contract with the National Aeronautics and Space Administration. Some data presented herein were obtained at the W.M. Keck Observatory, which is operated as a scientific partnership among the California Institute of Technology, the University of California and the National Aeronautics and Space Administration. The Observatory was made possible by the generous financial support of the W.M. Keck Foundation.

REFERENCES

Aragón-Salamanca, A., Ellis, R.S., Schwartzenberg, J.-M., & Bergeron, J.A., 1994, ApJ, 421, 27

Aragón-Salamanca, A., Ellis, R.S., & O'Brien, K.S., 1996, MNRAS, 281, 945

Bertin, E. & Arnouts, S., A&AS, 1996, 117, 393

Bruzual, A. G. & Charlot, S., 1993, ApJ, 405, 538

Bunker, A.J., Warren, S.J., Clements, D.L., Williger, G.M., & Hewett, P.C., 1999, in press

Cohen, J.G.,, Hogg, D.W., Pahre, M.A., Blandford,R., Shopbell, P.L., Richberg, K., 1998, ApJS, in press

Croom, S.M., & Shanks, T., 1998, MNRAS, in press

Dickinson, M., 1997, in *HST and the High Redshift Universe*, ed. N. Tanvir, A. Aragon-Salamanca & J.V. Wall, World Scientific

Djorgovski, S.G., Pahre, M.A., Bechtold, J., & Elston, R., 1996, Nature, 383, 234

Djorgovski, S.G., Banas, K.R., Odewahn, S.C, Gal, R.R., Pahre,M.A., De Carvalho, R.R., Desai,V., & Darling, J., 1997, BAAS 191.9507

Donahue, M., Boit, G.M., Gioia, I., Lupino, G., Hughes, J.P, & Stocke, J.T., 1998, ApJ, 502, 550

Ellingson, E., Yee, H.K.C., & Green, R.F., 1991, ApJ, 371, 49

Fowler, A.M. & Gatley, I., ApJ353, 33

Glazebrook, K., Blake, C., Economou, F., Lilly, S., & Colless, M., 1998, MNRAS in press

Hammer, F. et al., 1997, ApJ, 481, 49

Hall, P.B., Green, R.F., & Cohen, M., 1998, ApJS 119, 1

Hall, P.B., & Green, R.F., 1998, ApJ 507, 558

Hall, P.B., 1998, from the 13th Kingston Meeting on Theoretical Astrophysics: Galaxy Formation and Cosmic Star Formation History

Hu, E.M., Cowie, L.L, & McMahon, R.G., 1998, ApJLetters, 502, 99

Hutchings, J.B., 1995, AJ, 109, 928

Jaeger, K., Fricke, K.J., & Heidt, J., 1999, in "Bl Lac Phenomenon" Conference, in press

Kennicut, R. 1983, ApJ 272, 54

Kennicutt, R.C. & Kent, S.M., 1983, AJ, 88, 1094

Kennicutt, R.C., 1992, ApJ, 388, 31

Kirhakos, S., Sargent, W.L.W., Schneider, D.P., Bahcall, J.N., Jannuzi, B.T., Maoz, D., & Small, T.A., 1994, PASP, 106, 646

Larson, S., & McLean, I.S., 1997, ApJ, 491, 93

Lilly, S.J., Le Fevre, O., Hammer, F., & Crampton, D., 1996, ApJLetters, 460, L1

Malkan, M., Teplitz, H., & McLean, I., 1995, ApJ Letters 448, L5

Malkan, M., Teplitz, H., & McLean, I., 1996, ApJ Letters 468, L9

Mamon, G.A., Borsenberger, J., Tricottet, M., & Banchet, V., 1998, in 'The Impact of Near-Infrared Surveys on Galactic and Extragalactic Astronomy", ed. N. Epchtein (Dordrecht: Kluwer).

Mannucci, F., Thompson, D., Beckwith, S.V.W., & Williger, G.M ., 1998, ApJLetters, 501, L11 (MTBW98)

Matthews, K., & Soifer, B. T. 1994, in *Infrared Astronomy with Arrays: The Next Generation*, ed I. McLean (Dordrecht:Kluwer), 239

McCarthy et al., 1999, in preparation

McLean, I.S., 1994, in *Infrared Astronomy with Arrays: the Next Generation*, ed. McLean, I.S. (Kluwer)

McLean, I.S., Becklin, E.E., Brims, G., Canfield, J., Casement, L.S., Figer, D.F., Henriquez, F., Huang, A., Liu, T., Macintosh, B., & Teplitz, H., 1993, "The UCLA double-beam infrared camera system", in Proc. S.P.I.E., Vol. 1946, *Infrared Detectors and Instrumentation*, ed. Fowler, A., 513

McLean, I.S., Macintosh, B., Liu, T., Casement, L.S., Figer, D.F., Teplitz, H., Larson, S., Lacayanga, F., Silverstone, M., & Becklin, E.E., 1994, "Performance and results with a double-beam infrared camera", in Proc. S.P.I.E., Vol. 2198, *Instrumentation and Astonomy VI*, eds. Crawford, D.L. & Craine, E.R., 457

McLean, I.S., & Teplitz, H., 1996, AJ, 112, 2500

Moller, P.; Warren, S. J., 1998, MNRAS, 299, 66

Oemler, A., 1992, in *Clusters & Superclusters of Galaxies*, A Fabian ed., (Dordrecht: Kluwer), p.29

Oke, J. B., et al.,1995, P.A.S.P, 107, 375

Pahre, M.A. & Djorgovski, S.G., 1995, ApJL, 449, 1

Smail, I., Ivison, R.J., Blain, A.W., & Kneib, J.-P., 1998, ApJ, 507, 21

Stanford, S.A., Eisenhardt, P.R.M., Dickinson, M., 1995, ApJ, 450, 512

Steidel, C.C., Giavalisco, M., Pettini, M., Dickinson, M., & Adelberger, K.L., 1996, ApJ Letters 462, L17

Steidel, C.C., Dickinson, M., Meyer, D.M., Adelberger, K.L., & Sembach, K.R., 1997, ApJ, 480, 568

Steidel, C.C., Adelberger, K.L., Dickinson, M., Giavalisco, M., Pettini, M., & Kellogg, M., 1998, ApJ, 492, 428

Teplitz, H.I., Malkan, M.A., & McLean, I.S., 1998, ApJ 506, 519 (TMM98)

Teplitz,H.I., Gardner,J.P., Heap,S.R., & Malumuth,E.M., 1998, ApJL 507, L17

Teplitz, H.I., Malkan, M.A. & McLean,I.S., 1999, ApJ 514 (TMM99)

Thompson, D., Djorgovski, S, & Beckwith,S.V.W, 1994, AJ, 107 , 1

van der Werf, P.P., Bremer, M.N., Moorwood, A.F.M., Rottgering, H.J.A., 1997, IAU 186, 197

Yan, L., McCarthy, P. J., Storrie-Lombardi, L. J., & Weymann, R. J. 1998, ApJLeters, 503, L19

Yee, H.K.C., & Green, R.F., 1987, ApJ, 319, 28

Table 1. Filters in the UCLA 2-Channel Camera

Filter	central λ (μm)	$\Delta\lambda$ (μm)	Tranmission(%)
J	1.2	0.285	70
Pβ	1.28	0.01408	65
1.3095	1.3095	0.0130	78
H	1.65	0.3	≥ 70[a]
K$'$	2.1	0.35	≥ 70[a]

[a]manufacturer specification

Table 2. Broad Band Observations of $z \sim 1$ Targets

Field	date	itime (sec)	J 5σ	K′ 5σ
0107-025	08/04/95	2700	20.87	18.53
0122-003	08/05/95	3300	20.76	18.60
0246+009	10/19/96	3600	20.41	19.20
0308+002	10/27/96	2700	20.40	18.49
0333+321	10/19/96	3600	19.92	19.23
0447-092	10/19/96	3600	20.52	18.96
0500+019	10/19/96	4500	20.05	18.98
4c +22.21	03/13/96	3600	20.67	19.38
0743-006	03/13/96	3700	19.83	18.63
CBS 0076	10/27/96	3600	21.11	19.25
0903+474	03/13/96	3600	20.41	19.05
1050+542	03/12/96	3600	20.74	18.96
1231+163	03/12/96	3600	20.79	19.29
1235+112	03/12/96	3600	20.75	19.08
1244+324	05/20/95	3600	20.81	19.24
1306+296	05/06/96	3600	20.47	18.97
1307+296[a]	06/23/95	3600	20.61	19.07
KKC 70	06/25/95	3360	20.66	18.76
1331+170	05/20/95	3600	20.85	19.24
1331+2808	03/13/96	3600	20.72	19.28
1344+2818	03/12/96	2700	20.62	19.08
1502+105	05/20/95	3600	20.93	19.41
1540+110	05/20/95	3600	20.50	18.91
1608+4636	05/22/95	3600	20.76	19.13
1634+706	05/20/95	3600	20.73	19.09
1700+4744	05/22/95	4500	20.85	18.93
2145+067	08/04/95	3600	20.56	18.41
2350-0132	08/05/95	3600	20.65	18.67
2354+0048	08/05/95	3450	20.90	18.43
2358+0038	08/04/95	3600	20.95	18.89

[a]Close pair of Q1306+296 and Q1307+296 suggested surveyed area inbetween. This field is halfway between the two QSOs.

Table 3. Broad Band Photometry of QSOs

QSO	z_{em}	optical[a]	J	K′
0107-025	0.958	18.11	15.99	15.33
0122-003	1.007	17.0	15.78	14.50
0246+009	0.953	18.77	17.24	16.52
0308+002	0.955	20.49	19.8	17.4
0333+321	1.258	17.5	15.20	14.19
0447-092	0.946	18.5	16.61	15.33
PKS 0500+019	1.000	21.2	14.81	14.50
4c2221	0.951	19.5	17.49	15.73
0743-006	0.994	17.1	12.10	10.45
CBS 0076	0.945	17	15.54	14.83
PC 0903+474	0.948	18.61	17.15	16.31
1050+542	0.995	18.2	18.00	16.84
LBQS 1231+1627	0.999	18.80	17.09	17.30
LBQS 1235+1123	0.947	18.10	16.53	15.60
1244+324	0.949	17.2	16.34	15.40
1331+170	2.084	16.71	15.19	13.77
CCS 1331+2808	0.993	19.8	17.73	16.72
CCS 1344+2818	0.992	19.4	17.51	16.47
1502+105	1.00	17.79	16.59	15.56
1540+110	0.992	18	17.70	16.67
PC 1608+4636	0.951	19.15	17.93	16.57
1634+706	1.334	14.90	13.66	12.56
PC 1700+4744	0.994	18.07	16.187	15.89
2145+067	0.990	16.47	14.44	13.52
LBQS 2350-0132	0.993	17.39	15.334	14.76
LBQS 2354+0048	0.999	18.54	16.80	15.83
LBQS 2358+0038	0.949	18.73	16.54	15.72

[a]Optical magnitudes were taken from the NED catalog. Typically they correspond to B or V

Table 4. Narrow Band Observations of $z \sim 1$ Targets

Field	filter	date	itime (sec)	1σ SFR ($M_\odot yr^{-1}$)
0107-025	Pβ	10/20/96	14400	6
0122-003	Pβ	10/21/96	14580	6
0500+019	1.3095	10/20-21,23/96[a]	10620	8
1244+324	Pβ	05/22/95	11520	10
1331+170	Pβ	05/06/96	14580	6
1608+4636	Pβ	05/05-6/96	14580	6
1634+706	1.3095	08/06/95	11340	8
1700+4744	1.3095	08/07/95	12960	4
2145+067	1.3095	10/20-21/96	11340	10
2350-0132	1.3095	08/09/95	13500	6
2354+0048	1.3095	08/05/95	12960	4
2358+0038	Pβ	08/08/95	13860	6

Table 5. Observations of $z = 1.5$ Targets

Field	date	itime H (sec)	itime n.b.	H 5σ
87GB 1554+3526	01/30/94	600	2000	21.0
LBQS 2236-0023	07/18-19/94	1020	3240	21.5
CSO 190[a]	01/28/99	1680	4320	21.9
Q 1038+311[a]	01/28/99	1620	2640	21.3
Q 1147+339	01/28/99	840	2400	20.6
Q 1316+3111	01/28/99	1080	2400	21.0

[a]Due to observing constraints, these objects were chosen as signposts, even though they lie more than 1% from the center of the narrow band filter (both at $z = 1.45$).

Table 6. Narrow Band Detections at $z \sim 1$

Field	z	Δm	I	J	K′	SFR
2145+067	~ 0.995	1.2	:22.5 [a]	19.2	18.6	52.8
2350-0132	0.990	0.9	21.9	20.2	19.1	26.0

[a]magnitude is uncertain due to overlap with PSF of bright star

Table 7. Comparison of Narrow-Band Surveys

redshift	density 10^{-4} Mpc^{-3} (comoving)	3σ flux limit 10^{-16} ergs/cm^2/s	$< SFR >$ $M_\odot$/yr	Number of Galaxies	reference	notes on field selection
0.7–1.9	2	0.6	50	30	McCarthy 1999	random [a]
0.95–1.0	4.7	1.3	35	2	this work	QSO em.
1.5	< 40	:5.0	$\cdots$	0	this work	QSO em.
2.0–2.7	< 70	10	$\cdots$	0	Bunker 1999	DLA [d]
2.2–2.3	22.5	1.9	~ 40	2	van der Werf 1997	radio galaxies
2.2–2.5	0.33	3.4	250[b]	1	Thompson 1996	QSO em.
2.28–2.29	< 120	0.9	$\cdots$	0	Pahre 1995	QSO em.
2.3–2.4,0.89	9	4.8	70	18	MTBW98	Abs. line
2.3–2.5	60	1.0	50	5	TMM98[c]	Abs. line

[a]Slitless spectroscopy

[b]See Beckwith et al. 1998 for a discussion

[c]We have counted the density of objects from that survey with line fluxes greater than 1×10^{-16} ergs/cm^2/s.

[d]longslit spectroscopy

Table 8. J-band Number-Magnitude Counts

J mag.	N/deg^2/mag.	lower limit 1σ	upper limit 1σ
15.7500	155.153	80.9122	277.840
16.2500	310.305	202.940	463.519
16.7500	659.399	501.143	861.098
17.2500	775.764	603.932	991.038
17.7500	1318.80	1093.83	1586.05
18.2500	2404.87	2099.45	2710.29
18.7500	3646.09	3270.02	4022.15
19.2500	6206.11	5715.47	6696.75
19.7500	9301.09	8689.90	9912.28
20.2500	13702.9	12907.2	14498.5
20.7500	17970.0	17013.4	18926.6
21.2500	27714.0	26278.3	29149.8
21.7500	69312.5	64653.9	73971.2

Fig. 1.— J-band image of the 0107-025 field.

Fig. 2.— J-band number counts for the 0107-025 field. The error bars show the number counts for this field. The squares are the average of all J-band observations of z=1 fields

Fig. 3.— J-band image of the 2145+067 field. The Hα-emitter is circled and label "A".

Fig. 4.— J-band number counts for the 2145+067 field. The square points are the average of all J-band observations of z=1 fields

Fig. 5.— Broad-Narrow band color magnitude diagram for the 2145+067 field. The curved lines indicate the 99.5% confidence interval.

Fig. 6.— J-band image of the 2350-032 field. The Hα-emitter is circled and label "A".

Fig. 7.— Broad-Narrow band color magnitude diagram for the 2350-032 field. The curved lines indicate the 99.5% confidence interval.

Fig. 8.— J-band number counts for the 2350-032 field. The square points are the average of all J-band observations of z=1 fields.

Fig. 9.— LRIS spectrum of the candidate object in 2350-0132.

Fig. 10.— J-band number-magnitude counts for survey fields. The square points with error bars are the observed number counts. The + symbols are the counts from Bershady et al. 1998, and the solid line is the fit to the $J < 15$ counts presented in Mamon et al. 1998.

Fig. 11.— K-band number-magnitude counts for survey fields. The square points with error bars are the observed number counts. The + symbols are the counts from the literature as compiled in Gardner 1998.

Fig. 12.— Number of galaxies detected in the J band in the range $18 < J < 22$ with at least 3σ confidence in radial bins $5''$ wide. The error bars are the Poissonian error on the number of galaxies detected in each bin. The dotted line is the average number of galaxies per square arcminute in the total number counts in the same magnitude range.

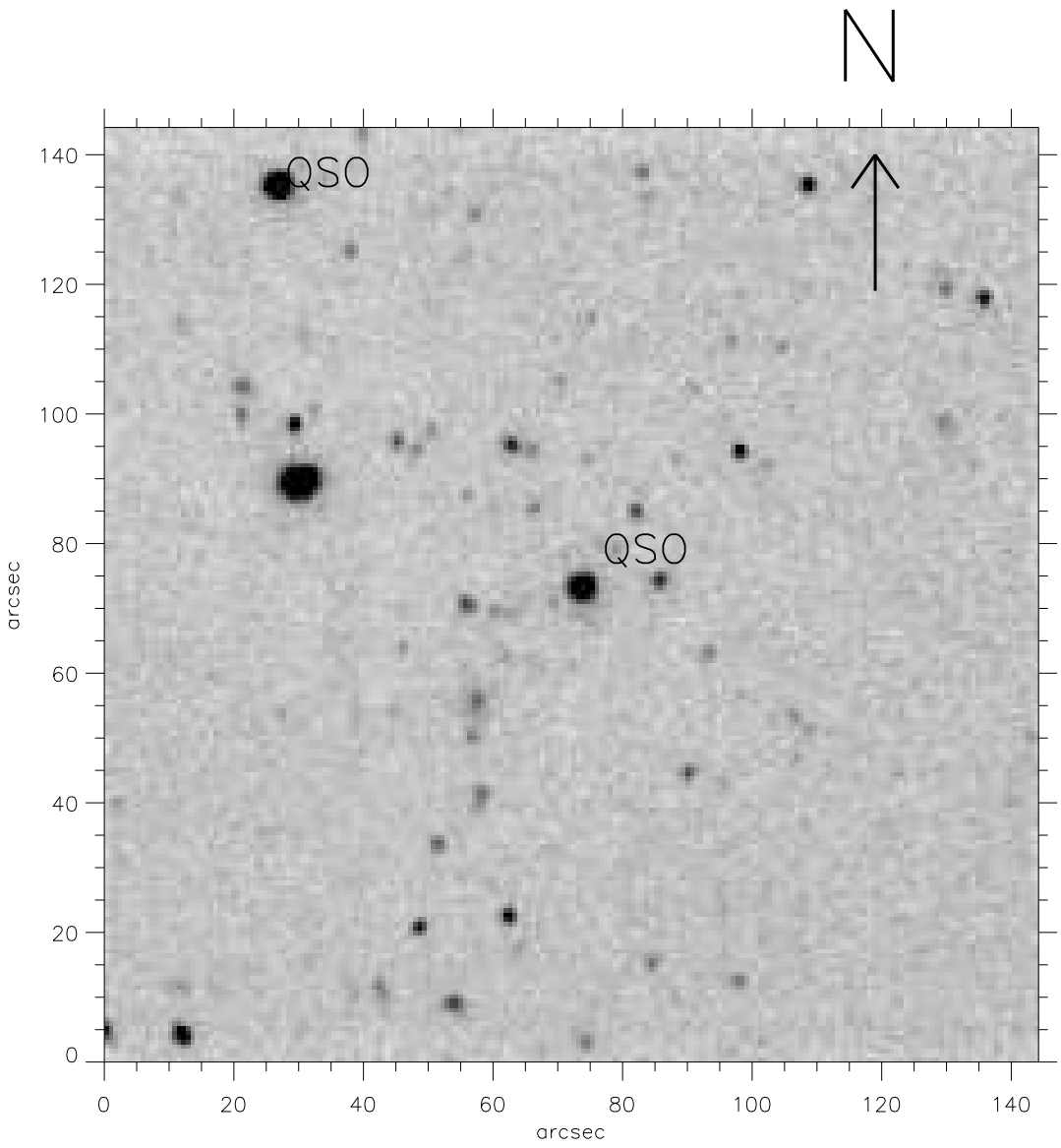
N
QSO
QSO
arcsec
arcsec
0
20
40
60
80
100
120
140

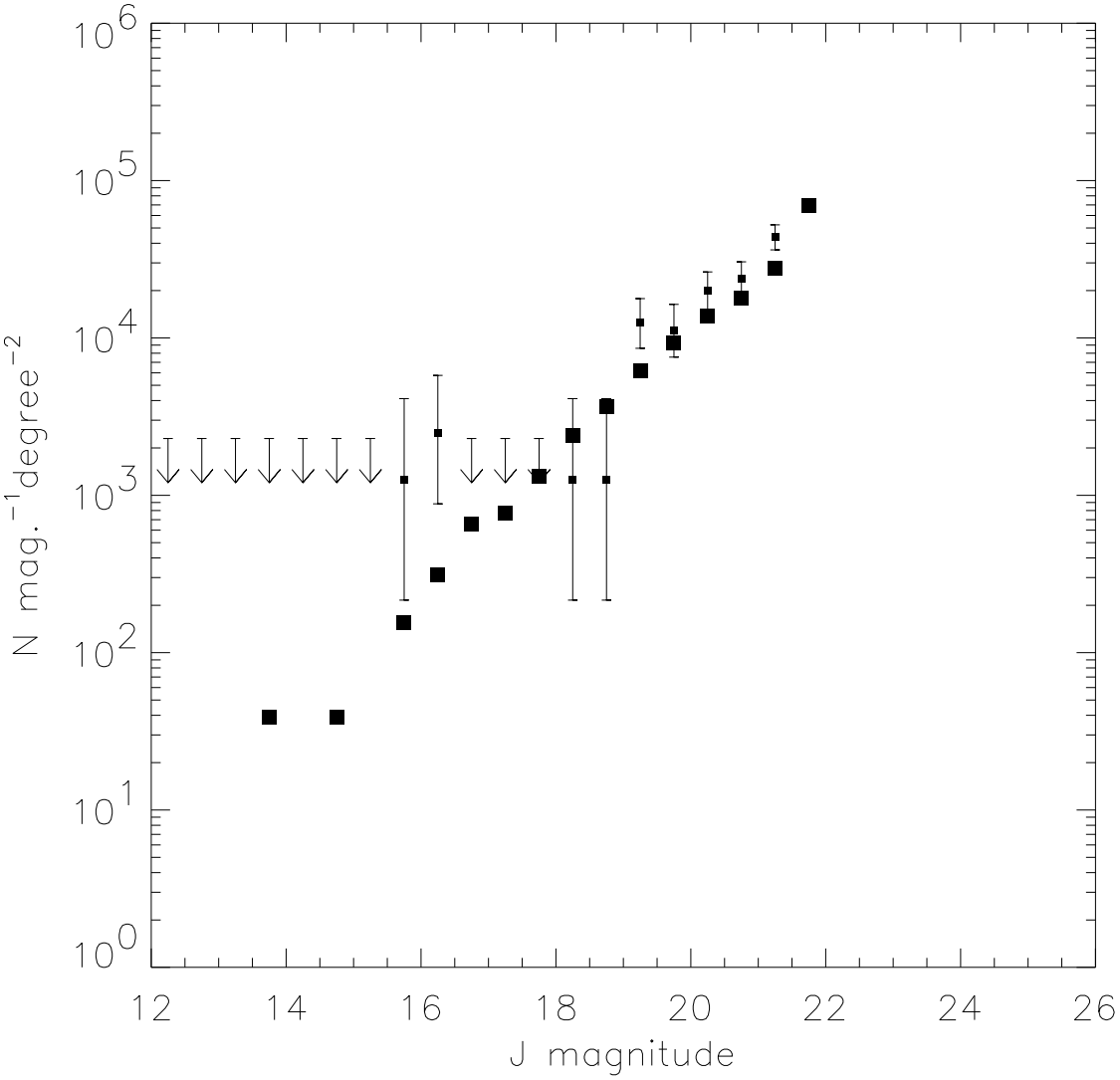
10^6
10^5
10^4
10^3
10^2
10^1
10^0
N mag.$^{-1}$degree^{-2}
12
14
16
18
20
22
24
26
J magnitude

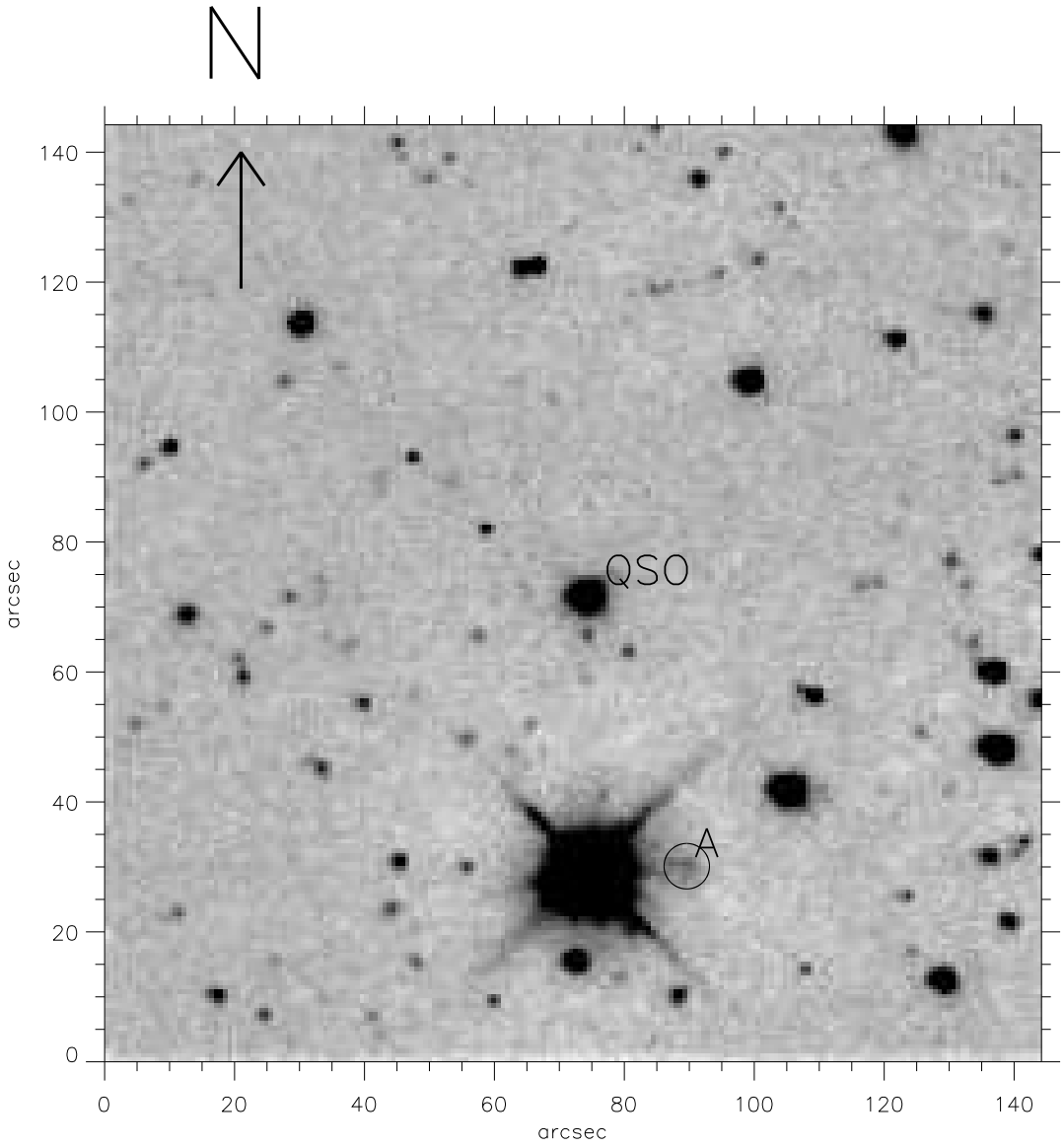
N
QSO
A
arcsec
arcsec
0
20
40
60
80
100
120
140

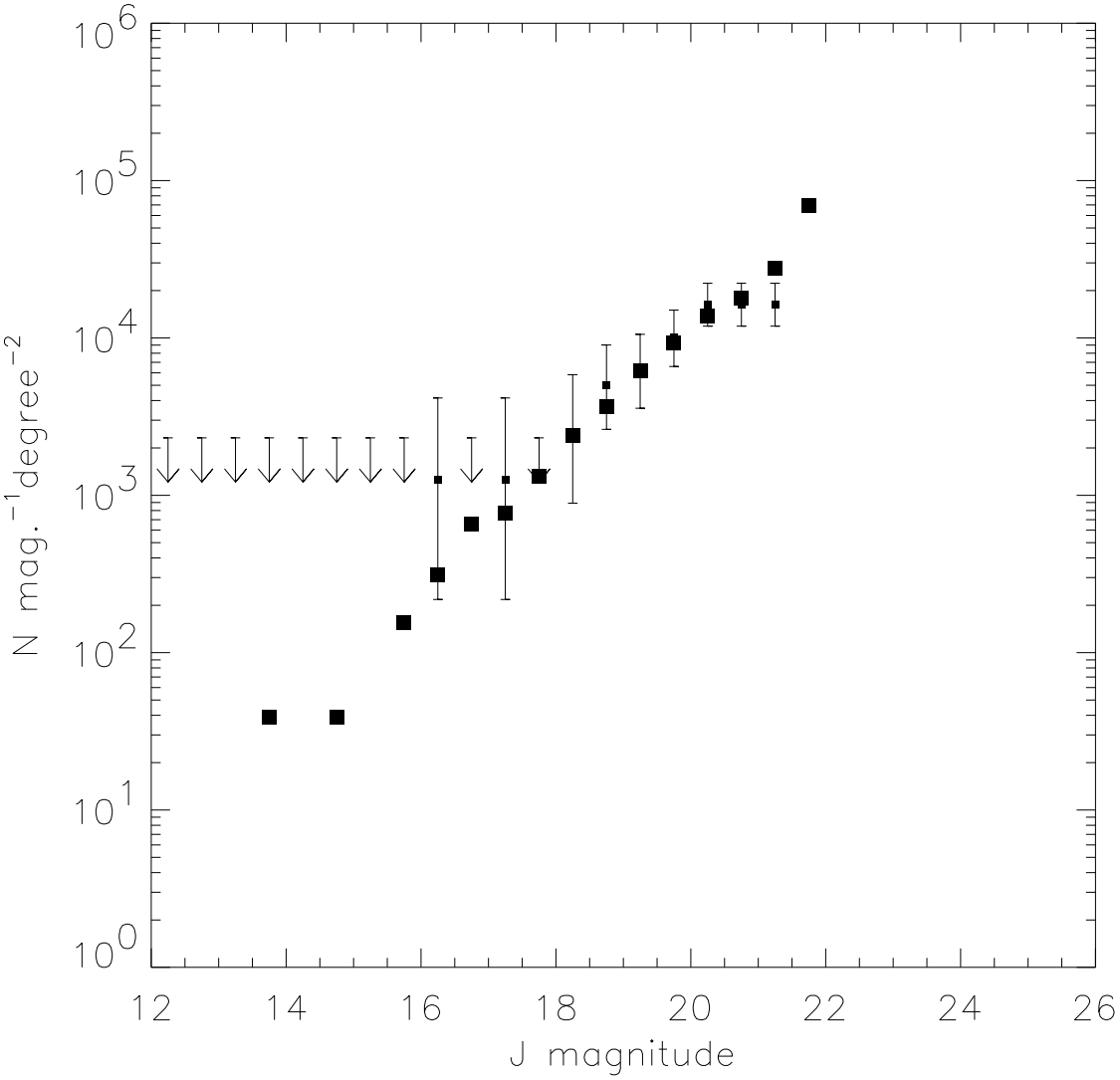
N mag.$^{-1}$degree^{-2}
J magnitude
10^0
10^1
10^2
10^3
10^4
10^5
10^6
12
14
16
18
20
22
24
26

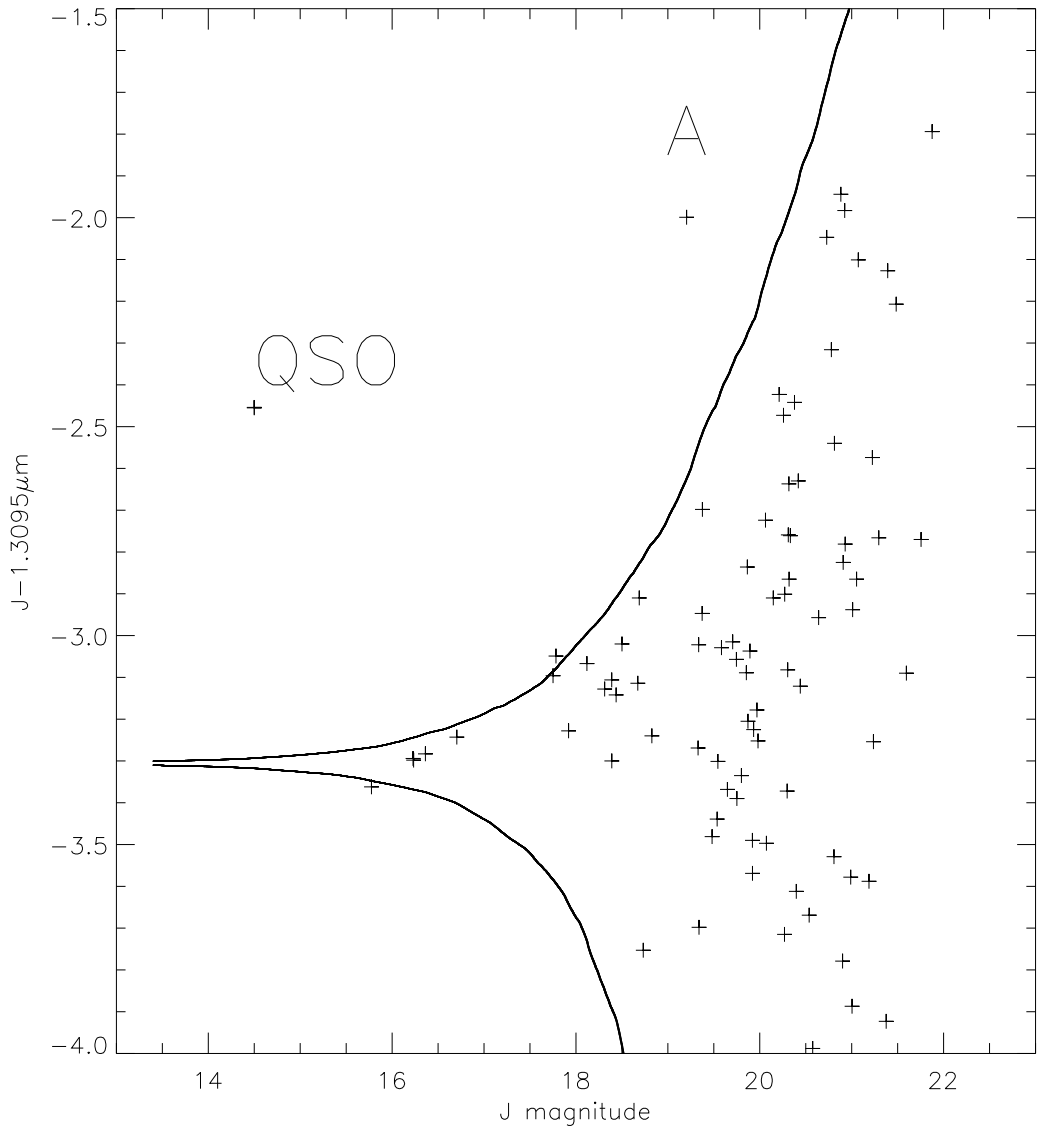
−1.5
−2.0
−2.5
−3.0
−3.5
−4.0
J−1.3095μm
14
16
18
20
22
J magnitude
QSO
A

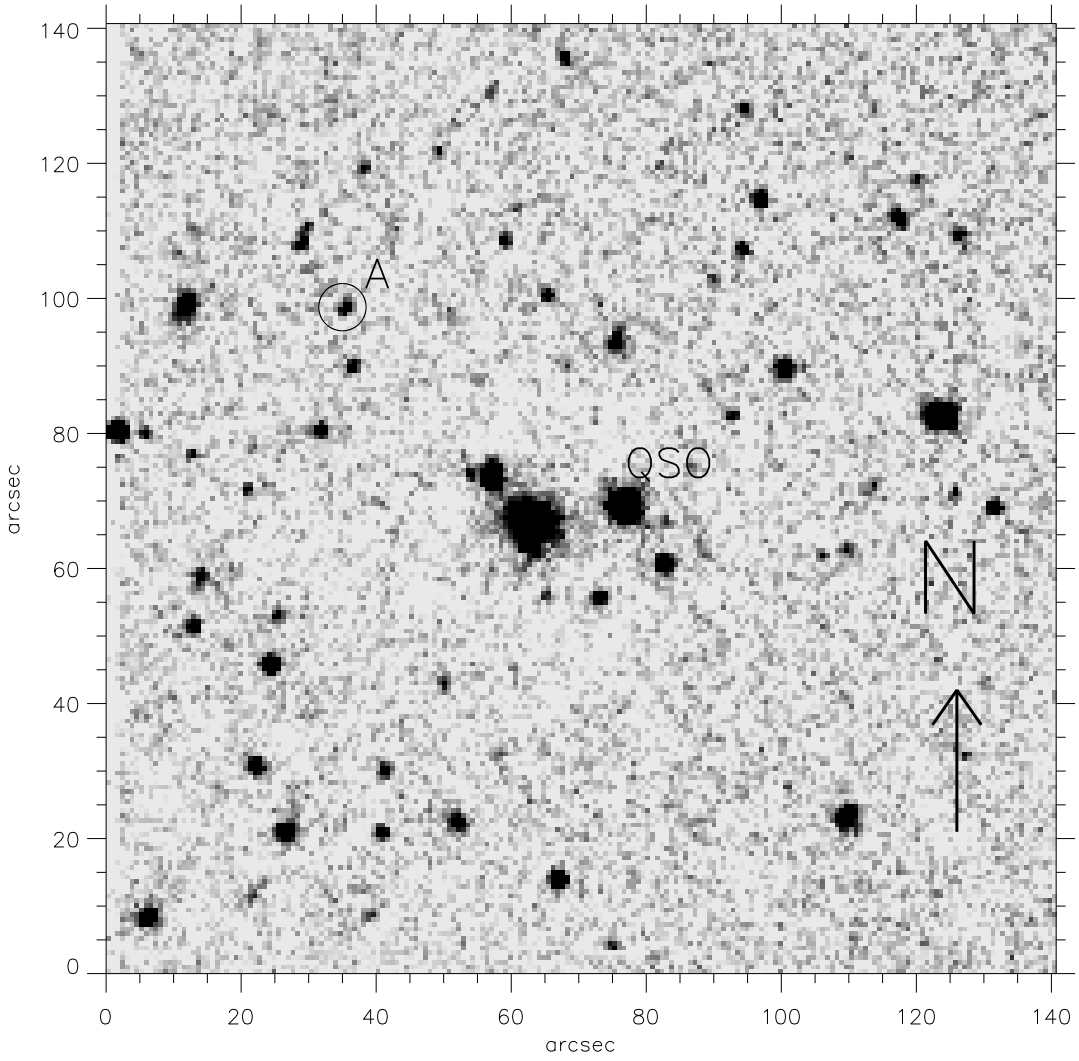
100 kpc at z=3.31
A
QSO
N
E
arcsec
arcsec
0
20
40
60
80
100
120
140

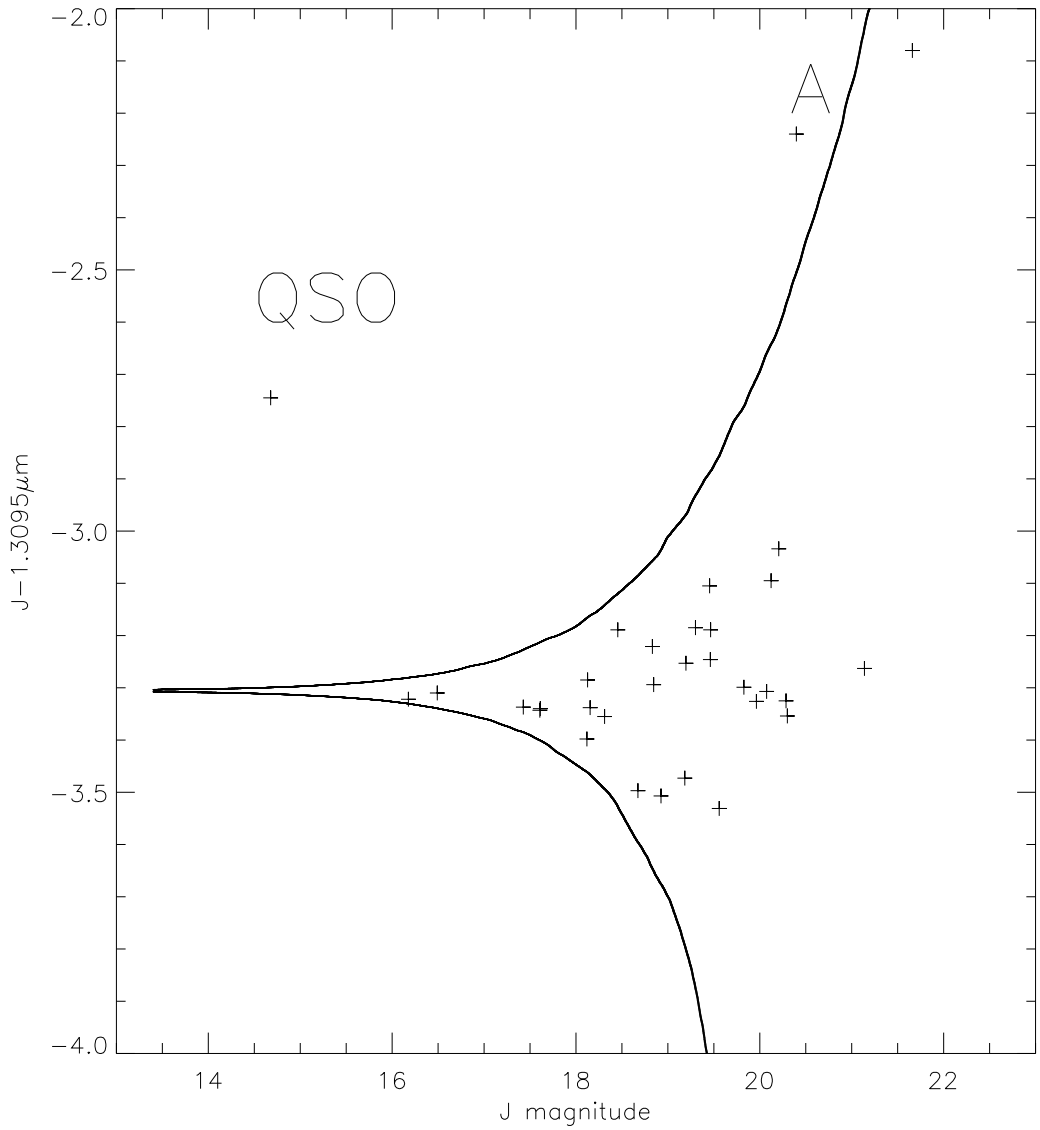
−2.0
−2.5
−3.0
−3.5
−4.0
J−1.3095μm
14
16
18
20
22
J magnitude
QSO
A

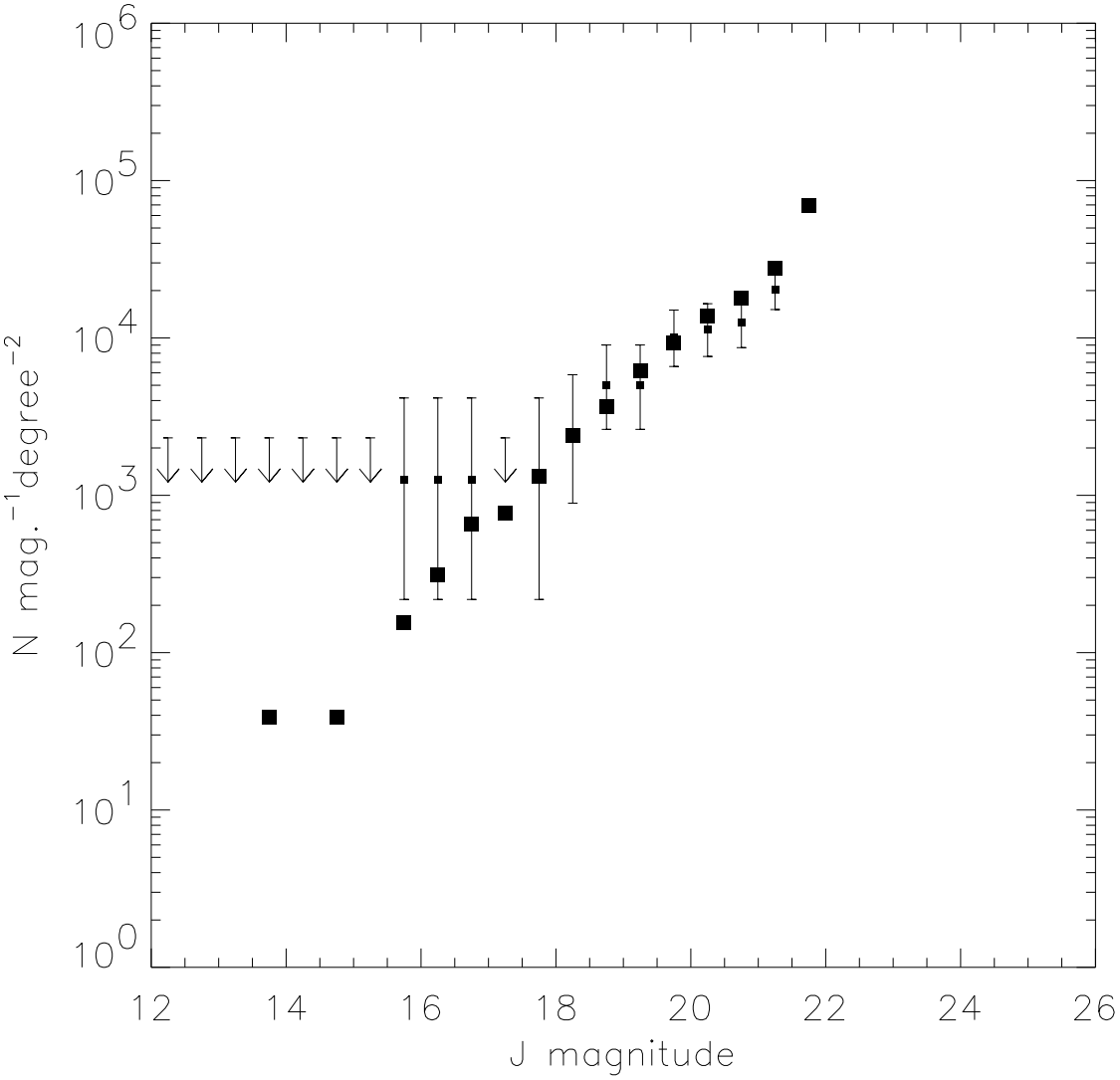
10^6
10^5
10^4
10^3
10^2
10^1
10^0
N mag.$^{-1}$degree^{-2}
12
14
16
18
20
22
24
26
J magnitude

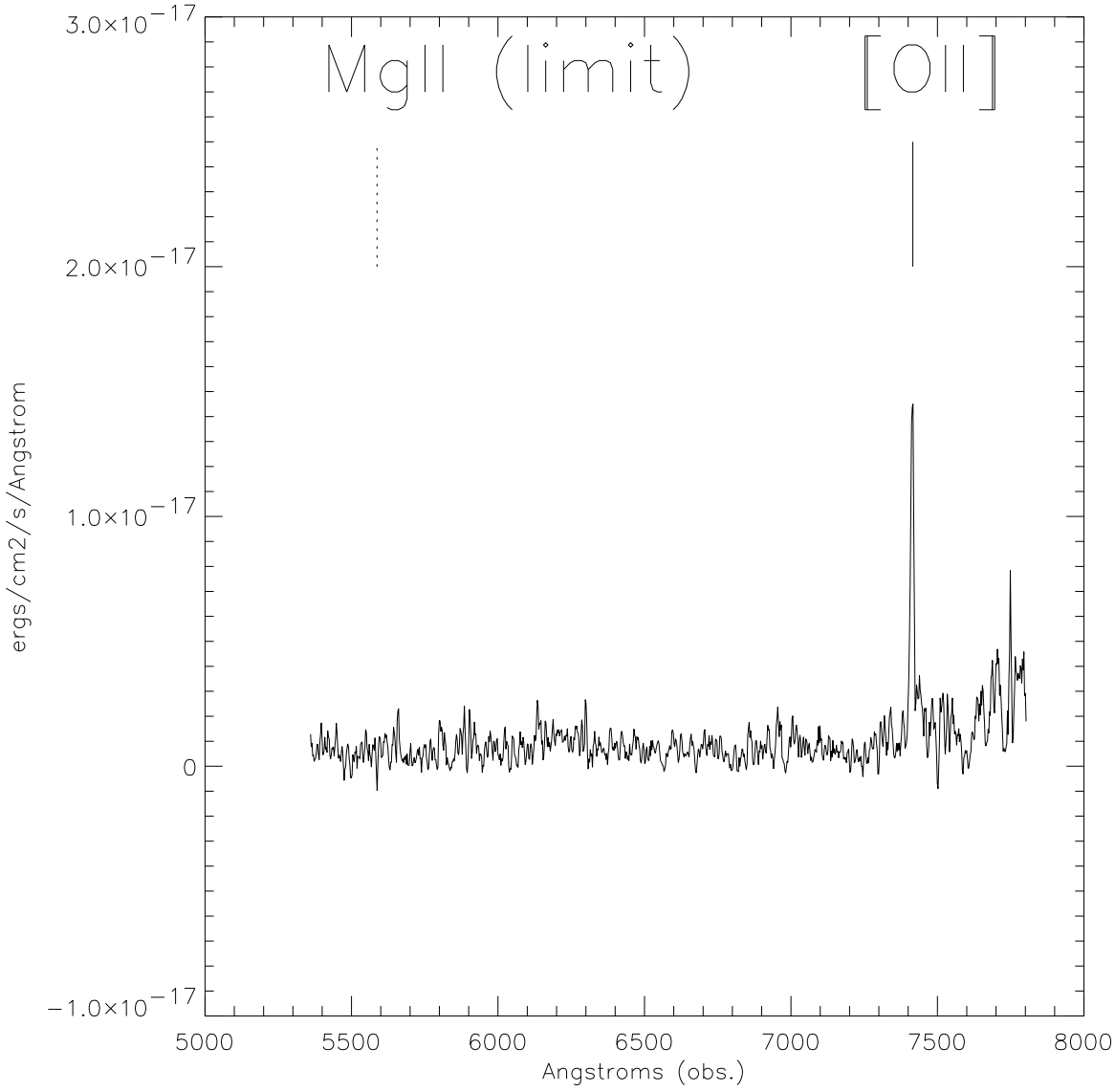
MgII (limit)
[OII]
3.0×10−17
2.0×10−17
1.0×10−17
0
−1.0×10−17
ergs/cm2/s/Angstrom
5000
5500
6000
6500
7000
7500
8000
Angstroms (obs.)

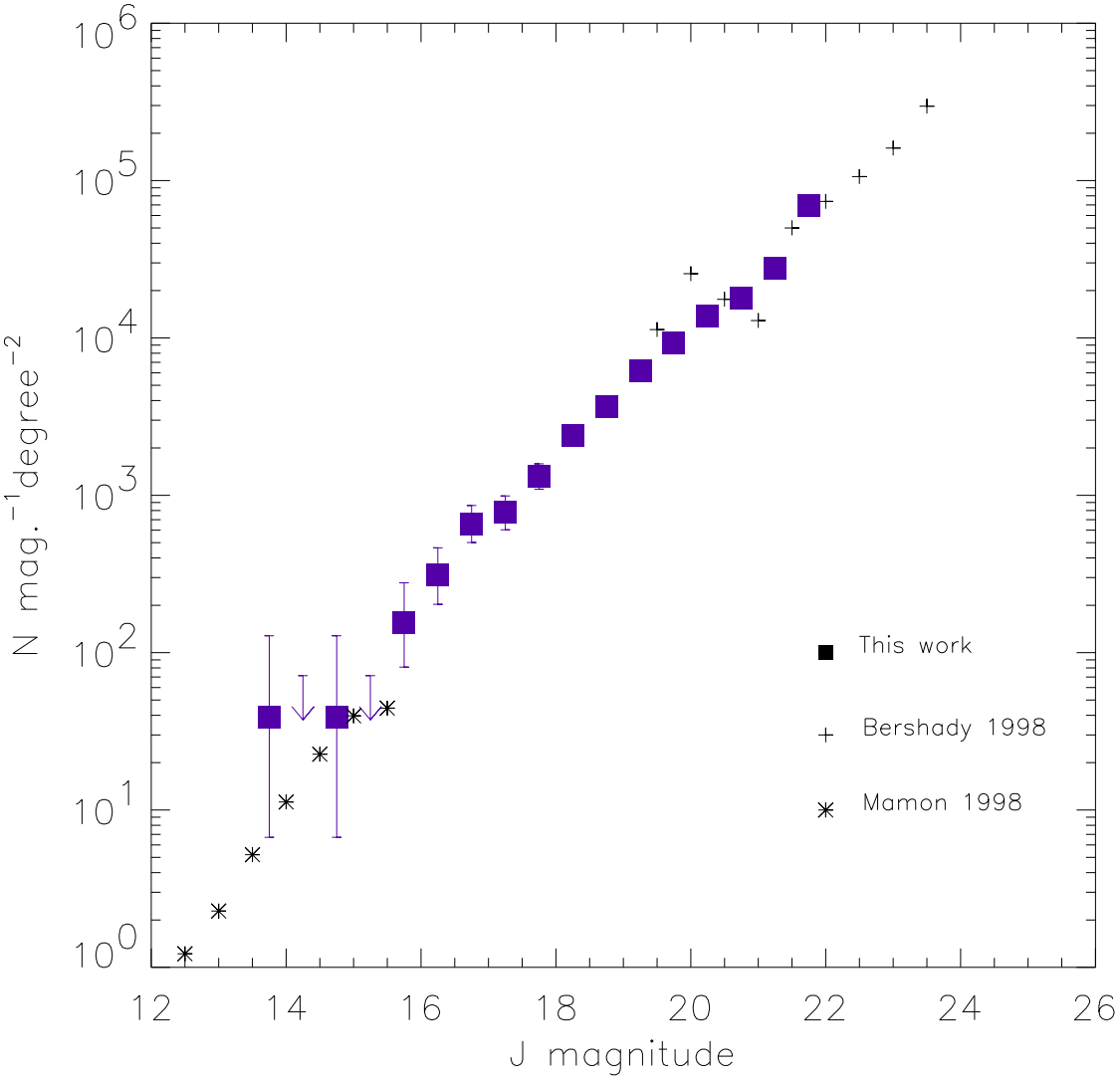
N mag.$^{-1}$degree^{-2}
J magnitude
This work
Bershady 1998
Mamon 1998

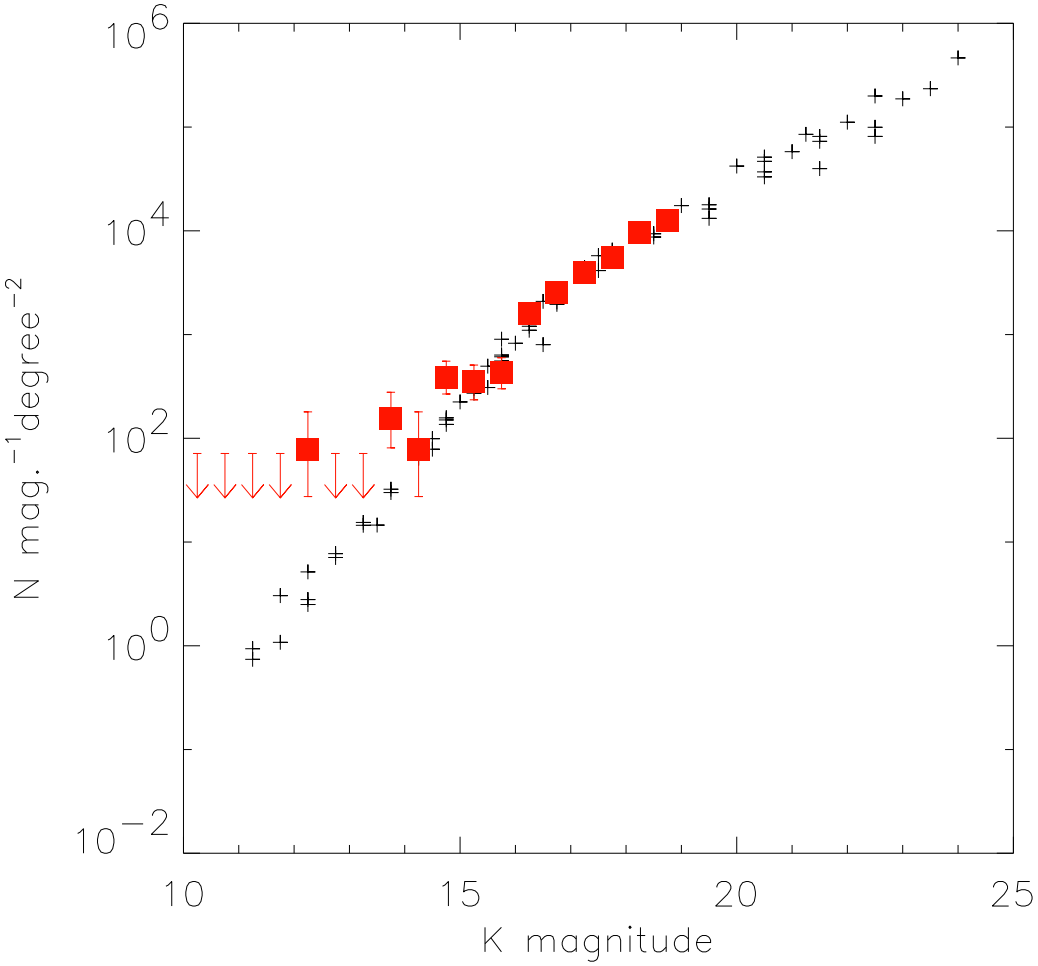
10^6
10^4
10^2
10^0
10^{-2}
N mag.$^{-1}$degree^{-2}
10
15
20
25
K magnitude

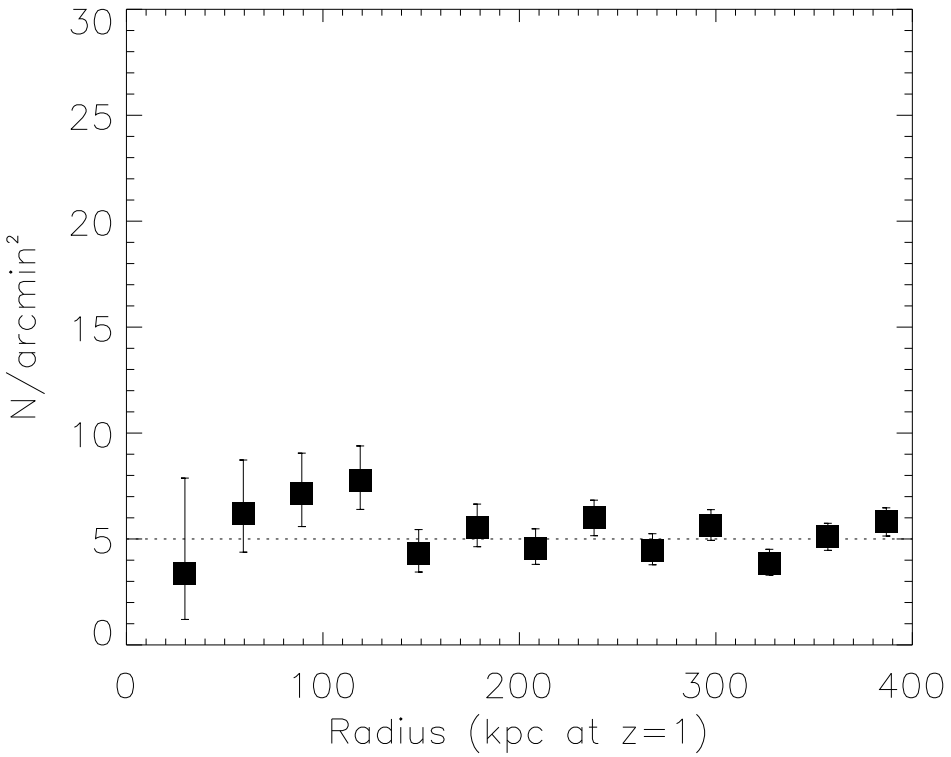
30
25
20
15
10
5
0
N/arcmin²
0
100
200
300
400
Radius (kpc at z=1)